

## Effects of Thickness Extension Mode Resonance Oscillation of Acoustic Waves on Catalytic and Surface Properties. IV. Activation of a Ag Catalyst for Ethanol Decomposition by Overtone Resonance Frequencies

N. Saito and Y. Inoue\*

Department of Chemistry, Nagaoka University of Technology, Nagaoka, 940-2188, Japan

Received: September 25, 2002; In Final Form: December 7, 2002

The effects of resonance frequencies of acoustic waves on catalytic and surface properties were studied. The overtone resonance frequencies of 3.5, 10.8, and 17.9 MHz were applied to a 100 nm thick Ag catalyst deposited on a ferroelectric z-cut LiNbO<sub>3</sub> crystal which generated thickness extension mode resonance oscillation (TERO). For ethanol decomposition, the TERO enhanced ethylene production without significant changes in acetaldehyde production for all the frequencies. The extent of catalyst activation strongly depended on the resonance frequency. In a low power region (<0.8 W), the TERO effect had a maximum at the middle of frequency, whereas in a high power region (>1.0 W), it increased in the order 3.5 > 10.8 > 17.9 MHz. The activation energy for ethylene production decreased remarkably in the presence of TERO, the extent of which strongly depended on the frequency. Laser Doppler measurements showed that with increasing resonance frequency, the number of standing waves increased markedly, whereas the amplitudes of the wave decreased considerably. The specific catalytic activity, defined as the activity enhancement per the density of wave, increased in a nonlinear manner with lattice displacement. The resonance frequency effects of TERO on catalyst activation are discussed.

### Introduction

In a series of the studies of acoustic wave resonance oscillations in heterogeneous catalysis,<sup>1–11</sup> we have demonstrated the effects of lattice vibration modes and the polarization fields on the catalytic activity and reaction selectivity. The thickness extension mode resonance oscillation (TERO) of bulk acoustic waves, generated by applying radio frequency power to a ferroelectric z-cut LiNbO<sub>3</sub> crystal, increased ethylene production markedly with a little influence on acetaldehyde production in ethanol decomposition over thin Ag and Pd film catalysts. Interestingly, the thickness shear mode resonance oscillation (TSRO) generated on an x-cut LiNbO<sub>3</sub> crystal had no ability to activate ethylene and acetaldehyde production.<sup>12</sup> Based on the lattice vibration and photoemission spectroscopic analyses,<sup>13</sup> it was clearly demonstrated that TERO induced large vertical lattice displacement that caused positive work function shifts, which were responsible for activity enhancement and selectivity changes. Furthermore, the TERO effects were shown to be strongly dependent on the polarized surfaces of the ferroelectric crystal: the catalyst activation and selectivity changes were different between a Ag catalyst deposited on a positively polarized surface (denoted here to as (+)Ag) and that deposited on a negatively polarized surface ((-)Ag).<sup>14</sup> The differences were associated with the findings that the positive work function shifts caused by the TERO were larger for (+)Ag than for (-)Ag. The polarization-dependent TERO effects on catalytic and surface properties also existed for (+)Pd and (-)Pd catalysts.<sup>7,15</sup>

In all the studies of TERO effects, we have used the first primary resonance frequency of 3.5 MHz only. For further development of acoustic wave excitation effects on metal

catalysts and for better understanding of the mechanism, it is of particular importance to clarify the effects of resonance frequency, that is, to see how different resonance frequencies affect the catalytic and surface properties.

There are two methods to obtain the different resonance frequencies of TERO. One is to employ overtone frequencies that appear as a series of resonance frequencies such as the first, the second, the third, and so on. The other is to change the crystal thickness of a ferroelectric crystal, since the frequency of TERO is inversely proportional to the thickness of a ferroelectric crystal. In the present study, the former method was chosen as a first step of research. In a preliminary investigation, we have found that the number and amplitudes of standing waves generated by TERO vary with resonance frequencies. In order to accurately examine the resonance frequency effects, it is considered beneficial to employ a ferroelectric crystal with a square shape, rather than that with a previously employed rectangular shape, since uniform distributions of standing waves would be more expected, because of a symmetric structure. The TERO effects with the first frequency of 3.5 MHz have already been reported for a ferroelectric crystal with a rectangular shape. However, because of the different crystal shape, it would be more convenient to show the results obtained for the first resonance frequency of a square shape ferroelectric crystal here, together with those for the second and third frequencies for better comparison of resonance frequency effects.

### Experimental Section

A z-cut LiNbO<sub>3</sub> single crystal was used as a ferroelectric substrate. The crystal (1 mm in thickness) was cut into a square shape of 14 mm × 14 mm. By assuming that the vibration mode of resonance oscillation is a thickness extension mode, fre-

\* Corresponding author.

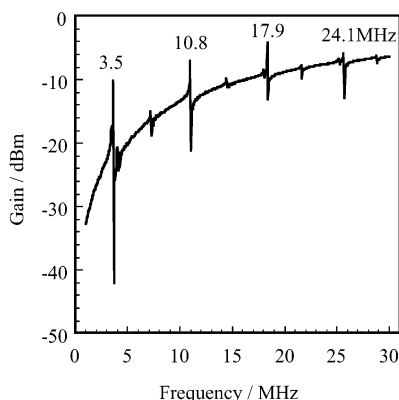


**Figure 1.** Overtone frequencies of TERO.

quency,  $f_r$ , is given by

$$f_r = \{(2n - 1)/2t\}(C_{33}^E/\rho)^{1/2}$$

where  $n$  is 1, 2, 3, integer,  $C_{33}^E$  is elastic constant,  $t$  is crystal thickness, and  $\rho$  is the density of a ferroelectric crystal.<sup>16,17</sup> For z-cut LiNbO<sub>3</sub> with  $t = 1$  mm, the calculated values were 3.7, 11.1, 18.4, and 25.9 MHz for  $n = 1, 2, 3,$  and  $4,$  respectively, Figure 1 shows the resonance lines observed by a network analyzer. The first, second, third, and fourth resonance lines appeared at 3.5, 10.8, and 17.9, and 24.1 MHz, respectively. The calculated values were close to the observed resonance lines. The observed resonance lines were exactly the same as those for a crystal with a rectangular shape of 14 mm  $\times$  44 mm, employed in previous studies.

A catalyst was prepared by depositing a Ag metal film on the front and back plane of the crystal by resistance heating of 99.999% pure Ag block in a vacuum. Radio frequency (rf) electric power was applied to a catalyst by the same method described elsewhere.<sup>6</sup> The catalytic reaction and the product analysis were reported previously.<sup>6</sup> Briefly, a closed gas-circulating reaction apparatus was used in a pressure of 4.0 kPa of ethanol vapor in the temperature range of 593–623 K. A catalyst was connected to Au wire and to BNC connectors that permitted the introduction of rf power.

Three-dimensional laser Doppler measurements were performed by a homemade apparatus, which was described elsewhere.<sup>6</sup>

## Results

Figure 2 shows the production of ethylene and acetaldehyde with reaction time in ethanol decomposition with TERO-on and TERO-off at three frequencies. The TERO at 3.5 MHz caused an immediate increase in ethylene production with a little enhancing acetaldehyde production. The high ethylene production was maintained until the TERO was turned off, and returned to a low level with TERO-off. The reaction behavior with TERO effects was analogous to those of the other two frequencies, but the extent of TERO effects was different. An activation coefficient,  $R$ , was defined by the ratio of activity with TERO-on to that with TERO-off as a measure of catalyst activation:  $R_e$  and  $R_a$  were denoted as the activation coefficient for ethylene and acetaldehyde production, respectively. At a frequency of 3.5 MHz, the value of  $R_e$  was 8.0, and  $R_a$  was 1.3. The TERO-on increased selectivity for ethylene production,  $S_e$ , from 62% (without TERO) to 90%. The TERO at 10.8 MHz caused a smaller activity enhancement for ethylene production, compared to that with 3.5 MHz:  $R_e$  was 4.4, and  $S_e$  was 85%. The TERO

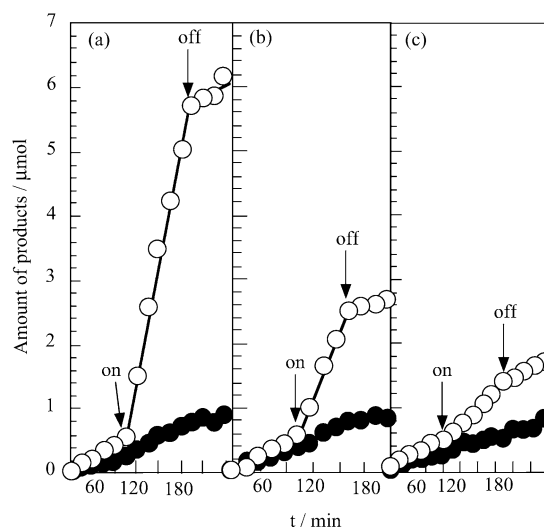


**Figure 2.** Changes in production of ethylene and acetaldehyde in ethanol decomposition with frequency of 3.5 (a), 10.8 (b), and 17.9 MHz (c) of TERO.  $\circ$ , ethylene;  $\bullet$ , acetaldehyde.  $T_r$  (for reaction temperature) = 613 K,  $J$  (for rf power) = 1.25 W,  $P_e$  (for pressure of ethanol) = 4.0 kPa.

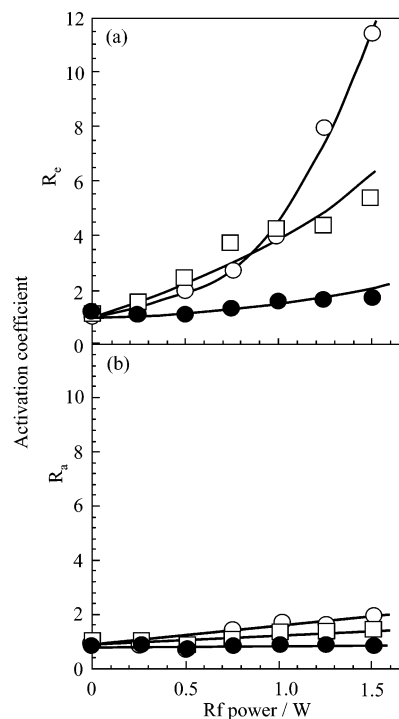
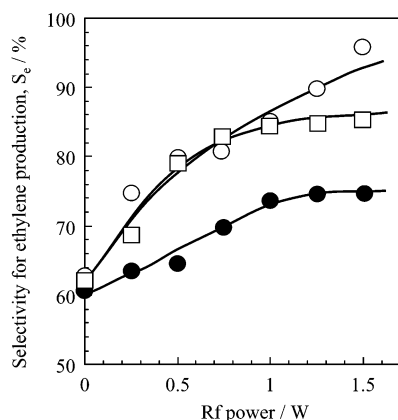


**Figure 3.** Activation coefficient for ethylene production,  $R_e$ , (a) and for acetaldehyde production,  $R_a$ , (b) as a function of rf power.  $\circ$ , 3.5 MHz;  $\square$ , 10.8 MHz;  $\bullet$ , 17.9 MHz.  $T_r = 613$  K,  $P_e = 4.0$  kPa.

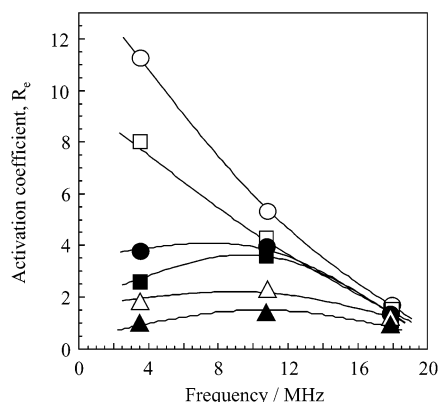
at 17.9 MHz induced much smaller activity enhancement:  $R_e$  was 1.4 and  $S_e$  was 75%.

Figure 3 shows  $R_e$  and  $R_a$  for the three frequencies as a function of rf power introduced to catalysts. With TERO-on at 3.5 MHz, the value of  $R_e$  increased gradually with increasing power, followed by a steep rise above 0.75 W and amounted to 11.4 at 1.5 W. On the other hand,  $R_a$  remained at around 2 or less over a power range. For 10.8 MHz,  $R_e$  was larger below 0.8 W and became much smaller above 1.0 W than  $R_e$  for 3.5 MHz. For 17.9 MHz, the enhancements of  $R_e$  were significantly small over a whole power range.

Figure 4 shows changes in  $S_e$  with rf power. The selectivity rises for ethylene production were considerably steep in a low



**Figure 4.** Increases in selectivity for ethylene production with rf power.  $\circ$ , 3.5 MHz;  $\square$ , 10.8 MHz;  $\bullet$ , 17.9 MHz.  $T_r = 613$  K,  $P_e = 4.0$  kPa.



**Figure 5.** Activation coefficient  $R_e$  as a function of frequency.  $\blacktriangle$ , 0.25;  $\triangle$ , 0.50;  $\blacksquare$ , 0.75;  $\bullet$ , 1.00;  $\square$ , 1.25;  $\circ$ , 1.50 W.  $T_r = 613$  K,  $P_e = 4.0$  kPa.

**TABLE 1: Changes in Activation Energy for Ethylene and Acetaldehyde Production with TERO**

product	rf power	activation energy/kJ mol <sup>-1</sup>			
		off	3.5MHz	10.8MHz	17.9MHz
ethylene	0.75		109	126	137
	1.00	140	100	115	121
	1.50		89	105	116
acetaldehyde	0.75		87	87	93
	1.00	93	87	87	93
	1.50		87	87	93

power region ( $<0.8$  W) and became slow with further increasing power. The selectivity changes were similar between 3.5 and 10.8 MHz up to 0.7 W, above which  $S_e$  for 3.5 MHz became larger than that for 10.8 MHz. The selectivity changes in 17.9 MHz occurred gradually with power. The largest selectivity was obtained at 1.5 W and 96, 85, and 75% for 3.5, 10.8, and 17.9 MHz, respectively.

The results shown in Figure 3 were re-plotted for various power to explicitly demonstrate a relationship between  $R_e$  and frequency. As shown in Figure 5, in a low power region below 1.0 W,  $R_e$  was the largest at a middle frequency of 10.8 MHz, whereas in a high power region above 1.25 W, the activity at 3.5 MHz increased markedly, and  $R_e$  became larger in the order  $3.5 > 10.8 > 17.9$  MHz.

Table 1 shows the activation energy for ethylene and acetylene production with TERO-off and TERO-on. The activation energy for ethylene production was 147 kJ mol<sup>-1</sup> with TERO-off. The TERO-on condition resulted in a decrease in a

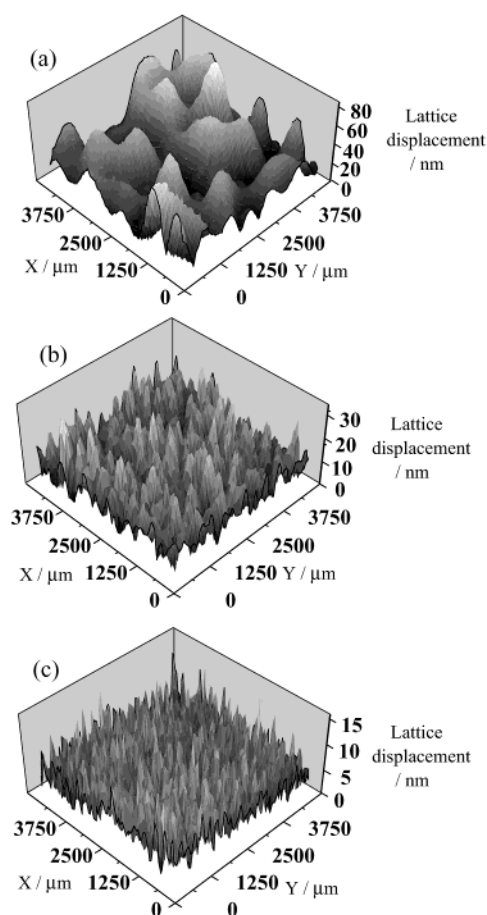


**Figure 6.** Three-dimensional images of standing waves generated at 3.5 (a), 10.8 (b), and 17.9 MHz (c).  $J = 1.0$  W,  $T_m$  (for measurement) = room temperature.

different way, depending on the rf power and resonance frequency. For 3.5 MHz, the activation energy dropped to 109 kJ mol<sup>-1</sup> at 0.75 W, 100 kJ mol<sup>-1</sup> at 1.0 W, and 89 kJ mol<sup>-1</sup> at 1.5 W. For 10.8 MHz, the activation energy was 126, 115, and 105 kJ mol<sup>-1</sup>, and, for 17.9 MHz, it was 137, 121, and 116 kJ mol<sup>-1</sup> at 0.75, 1.0, and 1.5 W, respectively. When compared at 1.5 W, the extent of activation energy drop was 40, 29, and 21% at 3.5, 10.8, and 17.9 MHz, respectively. It should be noted that the activation energy decreases became larger in the order  $3.5 > 10.8 > 17.9$  MHz. For acetaldehyde production, the activation energy of 93 kJ mol<sup>-1</sup> with TERO-off changed to be slightly low (87 kJ mol<sup>-1</sup>) for 3.5 and 10.8 MHz, but remained unchanged with 17.9 MHz.

Figure 6 shows the 3-dimensional (3D) laser Doppler images for the three frequencies at 1.0 W. Standing waves vertical to the surface appeared over the  $x$ - $y$  direction. As the frequency increased, a large number of the standing waves appeared, whereas the amplitudes of the waves changes appeared to be small. The standing waves represent lattice displacement vertical to the surface, and Figure 7 shows the distributions of lattice displacement for the three frequencies. At 3.5 MHz, broad distributions were observed. The largest lattice displacement,  $L_{max}$ , was 85 nm, and the average lattice displacement,  $L_{av}$ , was 30 nm. The full width at half-maximum (fwhm) was 40 nm. At 10.8 MHz, the distributions became considerably narrower:  $L_{max}$  and  $L_{av}$  were 30 and 9 nm, respectively. The value of fwhm was 12 nm. At 17.9 MHz, the distribution was much narrower:  $L_{max}$  and  $L_{av}$  were 17 and 4 nm, respectively. The value of fwhm was 5 nm. The magnitudes and distributions of lattice displacement became extremely small with increasing frequency.

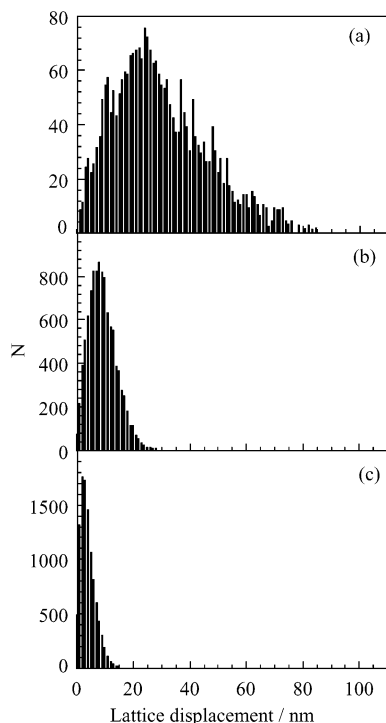


**Figure 7.** Lattice displacement distributions at 3.5 (a), 10.8 (b), and 17.9 MHz (c).  $J = 1.0$  W,  $T_m =$  room temperature.

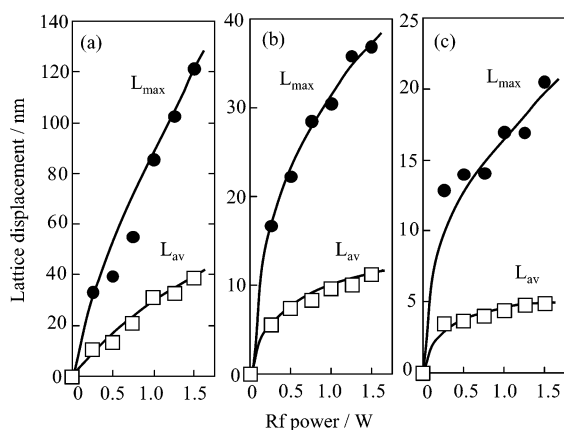


**Figure 8.** Changes in  $L_{max}$  (●) and  $L_{av}$  (□) at 3.5 (a), 10.8 (b), and 17.9 MHz (c) with rf power.  $T_m =$  room temperature.

Multiplying  $L_{max}$  by resonance frequency was around 300 nm MHz for three frequencies, which was nearly constant independent of frequency.

The number of standing waves per area,  $N_p$ , that is, the density of standing waves, was calculated. Figure 8 shows  $L_{max}$  and  $L_{av}$  as a function of rf power. Both  $L_{max}$  and  $L_{av}$  exhibited steep rises in a low power region, followed by gradual increases. Figure 9 shows correlations of  $N_p$  and  $L_{max}$  (and also  $L_{av}$ ) with frequency. An increase in frequency caused a considerable decrease in  $L_{max}$  ( $L_{av}$ ) and a marked enhancement of  $N_p$ .

## Discussion

The three frequencies showed similar behavior of catalyst activation for ethanol decomposition of a thin Ag film catalyst: ethylene production increased markedly with a little acceleration of acetaldehyde production. However, the extent of catalyst activation effects were significantly different among three resonance frequencies.  $R_e$  was larger at a middle frequency of 10.8 MHz in a lower power region ( $<0.8$  W), whereas it became

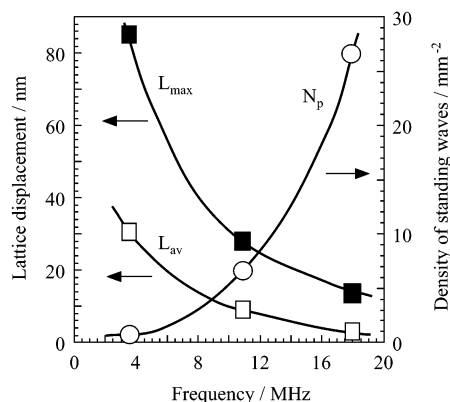


**Figure 9.**  $L_{max}$ ,  $L_{av}$ , and  $N_p$  as a function of frequency.  $J = 1.0$  W,  $T_m =$  room temperature.

larger in the order  $3.5 > 10.8 > 17.9$  MHz in a high power range ( $>1.0$  W). Furthermore, the extent of activation energy decreases became larger in the order  $3.5 > 10.8 > 17.9$  MHz. The frequency-dependent effects on the kinetic behavior of reaction are complex, and it is evident that they are associated with different changes in surface properties generated by respective TERO frequency. The standing wave patterns observed were quite different among the three frequencies. Since the standing waves correspond to vertical lattice displacement, the present results directly reflect changes in dynamic lattice displacement with frequency.

As shown in Figure 6, the lowest frequency produced markedly broad standing waves of large amplitudes, but the density of wave,  $N_p$ , was quite small. On the other hand, the highest frequency exhibited an extraordinary large number of standing waves with small amplitudes. The lattice displacement distributions became extremely narrower with increasing frequency. The quantitative correlation (Figure 9) showed that  $L_{max}$  decreased considerably whereas  $N_p$  increased remarkably. These changes can be analyzed as follows. The velocity of acoustic wave,  $v$ , is given by  $v = f\lambda$  where  $f$  and  $\lambda$  are the frequency of wave and wavelength, respectively. Because of  $\lambda = 2\pi L$  where  $L$  is the amplitude of wave,  $L$  is inversely proportional to  $f$ , that is,  $L = v/f$ . Multiplying  $L_{max}$  by  $f$  was found to be nearly constant (around 300 nm MHz at 1 W), independent of frequency, which indicates that a correlation of  $L = v/f$  is held where  $v$  is constant under the experimental conditions. If one assumes that one wave is approximated to a triangular cone shape such that the height is given by  $L$  and the half-radius of the bottom circle area of the cone is  $x$ ,  $N_p$  is expressed by  $N_p = 1/\pi x^2$ . Provided that the ratio of  $L/x$  is constant, that is,  $L/x = \alpha$ , independent of frequency,  $N = (\alpha^2/\pi v^2)f^2$ . This indicates that  $N_p$  increases in proportion to the square of frequency. As shown in Figure 10, experimental points were in good agreement with the derived equations. To confirm whether  $L/x = \alpha$  is constant, the shape of standing waves with different frequencies was compared at the same rf power. When  $L$  and  $x$  were normalized, differences in the waves among three frequencies are small, which showed the validity of the above-mentioned analysis. These results, furthermore, indicate that the shapes of standing waves are similar when the overtone frequency is changed.

The different activity enhancements with frequency can be explained by taking both the density,  $N_p$ , and magnitude,  $L$ , of lattice displacement into consideration. In a lower frequency regime,  $N_p$  was small, but  $L$  was large, whereas in a higher frequency regime, the situation was the opposite. As shown in Figure 5, in a low power, the effects of  $L$  remained within a

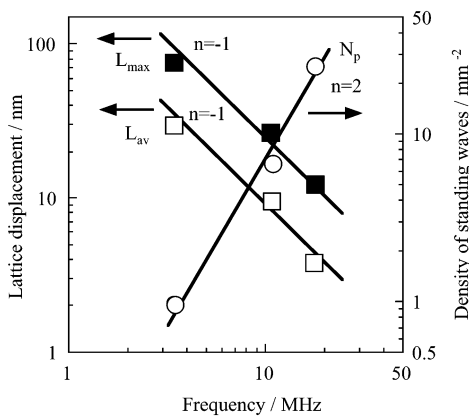


**Figure 10.** Logarithm plots of  $L_{\max}$ ,  $L_{\text{av}}$ , and  $N_p$  against frequency.

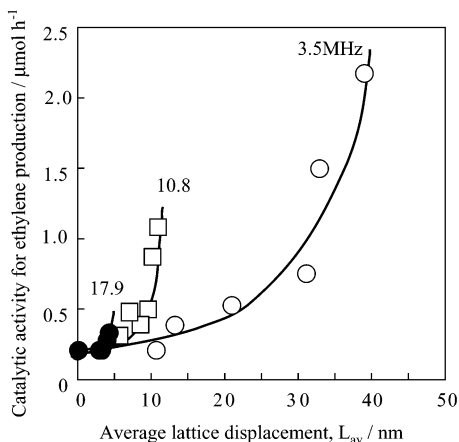


**Figure 11.** Correlations between catalytic activity for ethylene production and  $L_{\text{av}}$  for different frequencies.

small extent, and  $N_p$  also contributes to the activity. For the lowest frequency,  $N_p$  was too small, whereas for the highest frequency  $L$  was too low. In the case of the middle frequency at which both  $L$  and  $N_p$  are able to reach satisfactory levels together, the activity turns out to become the highest. This explains the appearance of a maximum in the correlation between activity and frequency at low power. On the other hand, at high power,  $L$  increased dramatically in lower frequency. Thus, the lattice displacement differences were so large that it was difficult for  $N_p$  to compensate the activity differences. Thus, it follows that the activity increased in the order  $3.5 > 17.9 > 10.8$  MHz, as observed at high power.

Figure 11 shows the activity for ethylene production as a function of  $L_{\text{av}}$ . For the three frequencies, the activity increased in a nonlinear manner with increasing  $L_{\text{av}}$ . The steepest rise of activity at 17.9 MHz and a gradual rise at 3.5 MHz were observed. When compared at the same  $L_{\text{av}}$  in a small lattice displacement region, the activity enhancement was higher in the order  $3.5 < 10.8 < 17.9$  MHz, which indicated that  $N_p$  was mostly responsible for the activity enhancement in this regime.

To separate the contributions of  $N_p$  and  $L$ , specific activity,  $V_{\text{sp}}$ , was defined as the total activity for ethylene production divided by  $N_p$ . Figure 12 shows a plot of  $V_{\text{sp}}$  vs  $L_{\text{av}}$  for the three frequencies. The plot provided a single line for the three frequencies. The nonlinear correlation indicated that the specific activity had nearly the second order with respect to  $L_{\text{av}}$ : the catalytic activity was enhanced efficiently at large lattice displacement.

We have previously performed photoelectron emission spectroscopic studies and have found that the TERO caused the

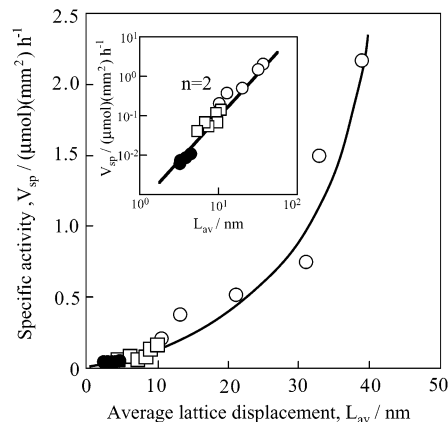


**Figure 12.** A correlation between specific activity for ethylene production and  $L_{\text{av}}$  at different frequencies. The inset showed a logarithm plot.  $\circ$ , 3.5 MHz;  $\square$ , 10.8 MHz;  $\bullet$ , 17.9 MHz.

positive shifts of threshold energy of photoelectron emission from Ag and Pd metal catalysts.<sup>13–15</sup> Based on the findings, a mechanism for TERO effects on work function was proposed. The work function of a transition metal is mainly determined by the barrier of an electric double layer that is formed by electrons spilled out from the topmost layer of a metal surface and positive charges remaining in the interior of the bulk metal.<sup>18,19</sup> Our assumption is that vertical lattice displacement by the TERO increases the density of “spill out” electrons, thus changing the electric double layer so as to cause positive work function shifts. Furthermore, the increased work function promotes the formation of weakly chemisorbed ethanol that has an orientation parallel to the metal surfaces,<sup>20</sup> thus enhancing ethylene formation through easier abstraction of HOH from the adsorbed ethanol.

In previous studies, the positive work function shifts were found to increase with increasing rf power,<sup>13–15</sup> which indicated that large vertical lattice displacement was responsible for large work function shifts. Because large vertical lattice displacement occurred at low resonance frequency, compared to high frequency, it is apparent that the low frequency was able to cause large positive work function shifts, and hence the TERO effects became larger in low frequency than in high frequency. This was a result observed for the TERO with low resonance frequency. Even if the magnitudes of lattice displacement are too small, it is unlikely that the TERO effects appeared significantly, no matter how large the density of standing waves is. In other words, even high density of lattice displacement leads to small TERO effects unless the vertical lattice displacement reaches a significant level.

To establish much larger catalyst activation by the TERO effects, the achievement of as large lattice displacement as possible at high resonance frequency is desirable. Previously, for ethanol oxidation on a Pd catalyst, we have demonstrated that a pulse TERO yields the high catalyst activation.<sup>21</sup> Thus, it is interesting to apply a pulse TERO of high resonance frequency to catalyst activation. Furthermore, an interesting comparative study is to employ ferroelectric crystals with different crystal thickness that permits us to change resonance frequency as the other method. The studies are in progress.

**Acknowledgment.** The work was supported by Grant-in-Aid of Scientific Research B from The Ministry of Education, Science, Sports and Culture. N.S. acknowledges Iketani Science and Technology Foundation.

## References and Notes

- (1) Ohkawara, Y.; Saito, N.; Inoue, Y. *Surf. Sci.* **1996**, 357/358, 777.
- (2) Saito, N.; Ohkawara, Y.; Watanabe, Y.; Inoue, Y. *Appl. Surf. Sci.* **1997**, 121/122, 343.
- (3) Ohkawara, Y.; Saito, N.; Inoue, Y. *Chem. Phys. Lett.* **1998**, 286, 502.
- (4) Saito, N.; Ohkawara, Y.; Sato, K.; Inoue, Y. *MRS symposium Proc.* **1998**, 497, 215.
- (5) Inoue, Y. *Catal. Survey Jpn.* **1999**, 3, 95.
- (6) Saito, N.; Nishiyama, H.; Sato, K.; Inoue, Y. *Chem. Phys. Lett.* **1998**, 297, 72.
- (7) Saito, N.; Sato, K.; Inoue, Y. *Surf. Sci.* **1998**, 417, 384.
- (8) Saito, N.; Nishiyama, H.; Sato, K.; Inoue, Y. *Surf. Sci.* **2000**, 454/456, 1099.
- (9) Saito, N.; Sakamoto, M.; Nishiyama, H.; Inoue, Y. *Chem. Phys. Lett.* **2001**, 341, 232.
- (10) Ohkawara, Y.; Saito, N.; Inoue, Y. *Solid State Ionics* **2000**, 136/137, 819.
- (11) Saito, N.; Nishiyama, H.; Inoue, Y. *Appl. Surf. Sci.* **2001**, 169/170, 259.
- (12) Saito, N.; Inoue, Y. *J. Chem. Phys.* **2000**, 113, 469.
- (13) Saito, N.; Inoue, Y. *J. Phys. Chem. B* **2002**, 106, 5011.
- (14) Saito, N.; Yukawa, Y.; Inoue, Y. *J. Phys. Chem. B* **2002**, 106, 10179.
- (15) Yukawa, Y.; Saito, N.; Nishiyama, H.; Inoue, Y. *J. Phys. Chem. B* **2002**, 106, 10174.
- (16) Ikeda, T. *Fundamental of Piezoelectricity*; Oxford University Press: New York, 1990; p 117.
- (17) Auld, B. A. *Acoustic Fields and Waves in Solids*; Wiley: New York, 1973; Vol. 2.
- (18) Lang, N. D.; Kohn, W. *Phys. Rev.* **1970**, B1, 4555.
- (19) Smith, J. R. *Phys. Rev.* **1969**, 181, 522.
- (20) Kratochwil, Th.; Wittmann, M.; Kupperts, J. *J. Elect. Spectrosc. Relat. Phenom.* **1993**, 64/65, 609.
- (21) Nishiyama, H.; Saito, N.; Izumi, K.; Inoue, Y. *J. Phys. Chem. B* **2002**, 106, 6538.